Water Air Soil Pollut (2023) 234:776
https://doi.org/10.1007/s11270-023-06805-8

Efficient Simultaneous Removal of Phosphorus and Copper from Wastewater by an Iron-Enhanced Dolomite Process

Hongyan Guan

Received: 14 July 2023 / Accepted: 5 December 2023 / Published online: 14 December 2023

Abstract The wastewater containing phosphorus (P) and copper (Cu) is produced in large quantities during manufacturing processes such as electroless plating of Cu. The focus of this work is to develop a green and cost-efficient process for the co-removal of P and Cu from wastewater. An iron-enhanced dolomite process was employed to treat the phosphate (PO_4–P) and copper contaminated water. The results showed that the co-removal of PO_4–P and Cu was feasible by adjusting parameters as reagent dosage, molar ratio, stirring time, and pH. Under the conditions of Ca/Fe molar ratio of 4:1, Fe/(P+Cu) molar ratio of 1:1, initial pH of 5.6~10.0, and stirring for 30 min, the removal rates of PO_4–P and Cu exceeded 99%. The mechanism research showed that the Fe ions was critical to the removal of PO_4–P, which mainly removed by forming insoluble amorphous precipitate. The raw $CaMg(CO_3)_2$ is susceptible to corrosion by Cu ions and resulting in the production of flaky particles, which have two-dimensional nanostructured. The two-dimensional nanostructured is conducive to increase the contact area of particles with ions in solution, improving the chemical reactivity and adsorption. The Cu ions are likely to be removed in the form of posnjakite. The process has the advantages of being green and cost-efficient, and has a good practical application prospect for the PO_4–P and Cu removal.

H. Guan (✉)
Shcool of Civil Aviation, Zhengzhou University of Aeronautic, Zhengzhou City, Henan Province, China
e-mail: guanhongyan321@163.com

Keywords Dolomite · Iron · Simultaneous Removal · Synergistic effect · Phosphate · Copper

1 Introduction

Phosphorus-containing wastewater is produced in large quantities during manufacturing processes such as electroless plating of copper (Cu), nickel (Ni), and tin (Sn) (Chen et al. 2020, Liang et al. 2019). The heavy metal ions inevitably remain in the wastewater. Lan et al. (2012) has reported that the residual Cu ion concentration in actual electroless copper-plating wastewater can reach 190 $mg{\cdot}L^{-1}$. Considering phosphorus (P) is the key element that caused eutrophication of water bodies, and excess Cu ion can cause pancreatic, skin, brain, and heart diseases; the emission control of them is critical to maintain water quality (Awual 2019, Badsha and Lo 2020). For example, the accept emission concentration of total phosphorus for municipal wastewater treatment plant (MWTP) effluent in China is less than 0.5 $mg{\cdot}L^{-1}$, and that of Cu is also restricted to 0.5 $mg{\cdot}L^{-1}$. The removal of P and Cu ion from wastewater is, therefore, crucial for the protection of the environment and human health.

Chemical precipitation is widely used for the removal of phosphate (PO_4–P) and heavy metals due to the high efficiency and easy operation (Clark et al. 1997, Fu and Wang 2011, Liu et al. 2011, Morse et al. 1998, Wang et al. 2015). In practice, salts of iron, and aluminum, such as $Fe_2(SO_4)_3$ and $Al_2(SO_4)_3$

are commonly combined with calcium hydroxide ($Ca(OH)_2$) for the removal of PO_4–P and heavy metals. However, the processes often involve the adjustment of acid or alkali, which may cause damage to implements and the environment. Due to the huge amount of processing, the cost of precipitants is also a big burden for manufacturers. Besides, the moisture content of the sludge generated by the processes is usually more than 90 wt%. Considering that dewatering is the key procedure for the sludge treatment prior to disposal, the high moisture content undoubtedly increases the cost (Qi et al. 2011). Therefore, in order to reduce the sludge disposal cost, the moisture content should be reduced as much as possible. Based on previous studies, the carbonate sediment has a lower moisture content than hydroxide sediment for the same heavy metal (Li et al. 2020). Hence, the carbonate precipitation may be a more appropriate approach than the traditional alkaline precipitation for the removal of PO_4–P and Cu.

Additionally, the chemical precipitation is ineffective to remove low-concentration contaminants. For example, there is no clear evidence that the P concentration can be reduced to 0.1 $mg{\cdot}L^{-1}$ or lower by chemical precipitation (Ramasahayam et al. 2014). Considering the adsorption is a commonly method to handle the low concentration of contaminants (Guo et al. 2017, Morse et al. 1998, Zhou et al. 2017), the combination of chemical precipitation and adsorption is likely to be a good technical route.

In wastewater treatment, calcite has recently shown excellent performance and application prospects due to its distinctive characteristics of precipitation and adsorption in different situations. For example, Lei et al. (2019) activated $CaMg(CO_3)_2$ particles by using H^+ generated near the anode in the electrochemical process. Along with the consumption of H^+ by $CaMg(CO_3)_2$ particles, Ca ions were continuously released into the flowing solution and a large amount of P can be removed by the free Ca ions. Zhang et al. (2018) investigated the P removal by in situ generated ferrous ions Fe(II) and inferred that PO_4–P removal occurred via co-precipitation and adsorption. Dolomite ($CaMg(CO_3)_2$), like calcite, is also a cheap and environmentally friendly material with a wide range of sources, rich in calcium, magnesium, and carbonate ions. However, at present, there are few literature reports on the removal of pollutants in wastewater by dolomite. Therefore, based on dolomite, developing a green and cost-effective process to simultaneously remove PO_4–P and Cu in wastewater is of great significance to the electroless plating industry.

In this work, the Fe(II) ion coupling dolomite process was developed to handle the PO_4–P and Cu solution. Firstly, the effects of key factors, including stirring time, initial pH, and the molar ratio of dolomite-Ca to Fe(II) (Ca/Fe) on the removal of PO_4–P and Cu, were investigated. Then the removal mechanism was discussed by the design experiments.

2 Experimental Section

2.1 Materials

Dolomite ($CaMg(CO_3)_2$), calcium hydroxide ($Ca(OH)_2$), ferrous sulfate heptahydrate ($FeSO_4{\cdot}7H_2O$), ferric sulfate hydrate ($Fe_2(SO_4)_3{\cdot}H_2O$), anhydrous copper sulfate ($CuSO_4$), and trisodium phosphate dodecahydrate ($Na_3PO_4{\cdot}12H_2O$) were purchased from Sinopharm Chemical Reagent Co., Ltd. (Shanghai, China). All of the abovementioned chemicals were analytical grade (purity > 99%) and used as received. The pH adjusters were sodium hydroxide solution (NaOH) and sulfuric acid solution (H_2SO_4), respectively, both with the concentration of 30%. Ultrapure water was produced by an ultrapure water device with the electrical conductivity of 18.2MΩ·cm.

2.2 Procedure

Firstly, the effect of (Ca+Fe)/(P+Cu) molar ratio was investigated with conditions: the equimolar $CaMg(CO_3)_2$ and $FeSO_4{\cdot}7H_2O$ were added into 200 mL solution with the initial concentrations of 1 mM PO_4–P (30.9 $mg{\cdot}L^{-1}$), 1 mM Cu (63.5 $mg{\cdot}L^{-1}$) ions, and stirred for 30 min with 500 rpm. The molar ratios of (Ca+Fe)/(P+Cu) were set at 1:1, 2:1, 6:1, and 10:1. The initial pH at 7.6.

Then, the effects of Ca/Fe molar ratio on the removal of PO_4–P and Cu ions were investigated by setting the molar ratio at 1:1, 2:1, 4:1, 8:1, and 12:1, respectively. The initial concentrations of PO_4–P and Cu were controlled at 1 mM. In the batch experiments, the dosage of $FeSO_4{\cdot}7H_2O$ was fixed at 1mM and the stirring time was 30 min and the speed was set at 500 rpm. For the Fe/Ca cases, the dosage of $CaMg(CO_3)_2$ was fixed at 1 mM with the same stirring time and speed. The initial pH of the experiment was fixed at 5.6.

Hereafter, 0.4 mmol $CaMg(CO_3)_2$ and 0.4 mmol $FeSO_4{\cdot}7H_2O$ were added into 200-mL solution with the concentrations of 1 mM PO_4–P and 1 mM Cu ions. The initial pH was fixed at 7.6. The solution was stirred in an open beaker at 25 ℃ at a speed of 500 rpm. Two milliliters of sample was taken out at 10, 20, 30, 40, 50, and 60 min, respectively.

Finally, the effect of pH on the removal of PO_4–P and Cu ions was investigated by changing the initial pH at 3.0, 4.0, 5.1, 5.6, 6.4, 7.6, 10.6, 11.7, and 12.4. The dosages of $CaMg(CO_3)_2$ and $FeSO_4{\cdot}7H_2O$ were controlled at 1 mM, respectively. The concentrations of PO_4–P and Cu ions were both set at 1 mM. The stirring time and speed were fixed at 30min and 500 rpm, respectively. In order to reveal the removal mechanism of PO_4–P and Cu ions, designed experiments were carried out and specific experimental conditions were shown in relevant sections.

2.3 Characterization

The concentration of PO_4–P was determined by molybdenum blue spectrophotometric method using a UV spectrophotometer (DR 5000, HACH, USA) at 700 nm. Inductively coupled plasma optical emission spectrometer (ICP-OES, OPTIMA 8300, USA) was used to detect the concentration of Cu. The phase was determined by X'Pert-Pro MPD diffractometer (Netherlands PANalytical) with a Cu Kα X-ray source. The morphology of sample was observed with SEM 107 (JSM-5610LV, JEOL, Ltd., Japan). The morphology and surface elements were analyzed by a thermal field emission high-resolution scanning electron microscope (NOVA Nano SEM 430+EDS, FEI, USA). X-ray photoelectron spectroscopy (XPS, PHI Quantera SXM, ULVAV-PHI, Japan) was employed to probe the chemical valence of elemental irons. The pH was measured with a portable multi-parameter analyzer (HACH, HQ30D, USA).

The removal rate was calculated by Eq. (1):

$$R = \frac{C_i - C_f}{C_i} \times 100 \quad (1)$$

where R is the removal rate (%); C_i is the initial concentration ($mg{\cdot}L^{-1}$); C_f is the residual concentration in solution.

3 Results and Discussion

3.1 Effect of (Ca+Fe)/(P+Cu) Molar Ratio

The effect of the dosage of $CaMg(CO_3)_2$ and $FeSO_4$ is investigated by fixing Ca/Fe at 1:1 and the results are shown in Figure 1. As the molar ratio of (Ca+Fe)/(P+Cu) increases, the removal rates of PO_4–P and Cu both rise. The removal rate of PO_4–P increases from 90.9% to nearly 100.00% with the molar ratio increases from 1:1 to 2:1, while the removal rate of Cu increases from 72.4 to 75.8%. As the molar ratio reaches 10:1, the Cu removal rate increases to 96.4%. It indicates that the dosage of $CaMg(CO_3)_2$ and $FeSO_4$ is important to the removal of Cu.

3.2 Effect of Ca/Fe Molar Ratio

Figure 2 shows the effect of the molar ratio of Ca and Fe on the removal rates of PO_4–P and Cu. The effect of Ca/Fe molar ratio is shown in Figure 2 a. It can be seen that the $CaMg(CO_3)_2$ has a positive effect on the removal of PO_4–P and Cu ions. In particular, the $CaMg(CO_3)_2$ has more significant effect on the Cu removal, for example, the removal rate of Cu increases from 38.7 to 97.1% with the Ca/Fe molar ratio increases from 1:1 to 12:1. It is demonstrated that the $CaMg(CO_3)_2$ is vital for the removal of Cu

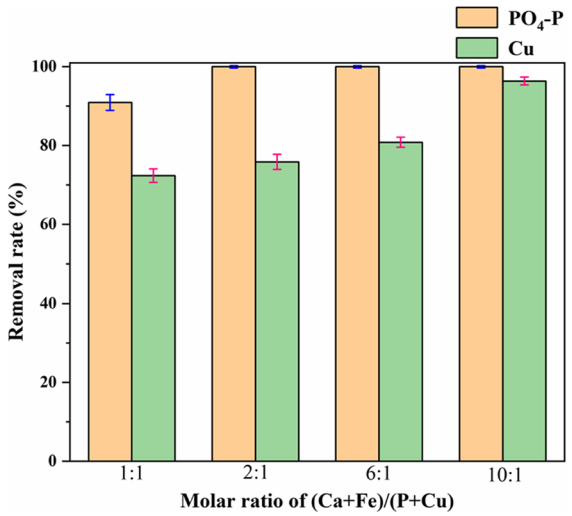

Figure 1 Effect of the (Ca+Fe)/(P+Cu) molar ratio on the removal rate of PO_4–P and Cu (Ca/Fe=1:1) (Initial pH at 7.6; Cu/P =1:1)

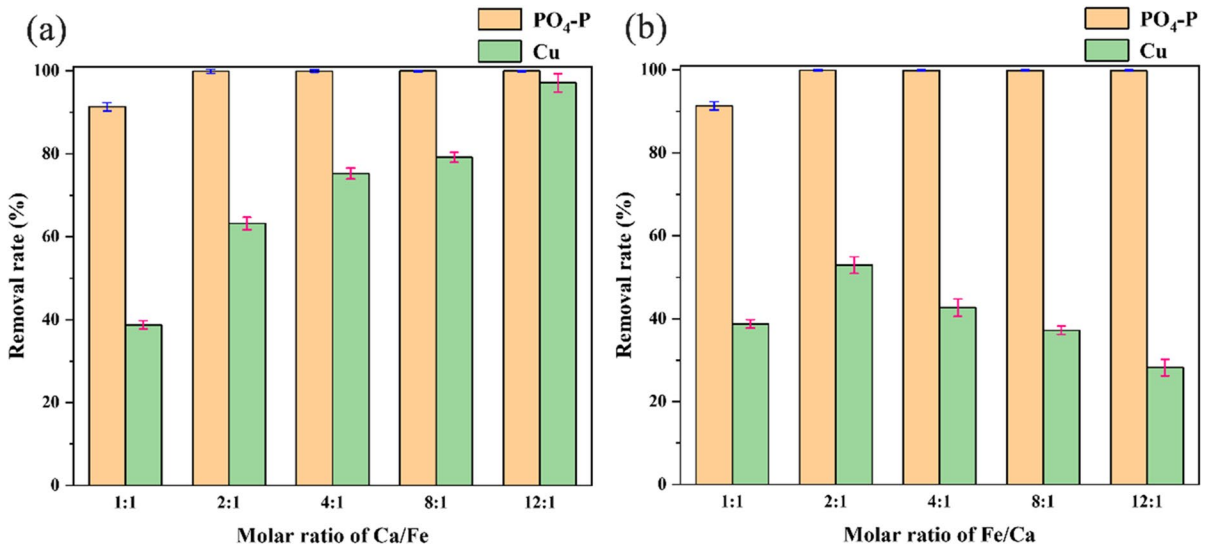

Figure 2 Removal rates of PO_4–P and Cu versus the molar ratio of Ca/Fe (**a**) and Fe/Ca (**b**)

ions in the process. Figure 2 b shows the effect of Fe/Ca molar ratio on the PO_4–P and Cu ion removal. In the case of PO_4–P removal, the $FeSO_4$ always has a positive effect. But for Cu ions, the removal rate firstly increases from 38.7 to 52.9% with the Fe/Ca molar ratio increases from 1:1 to 2:1, and then decreases from 52.9 to 28.2% as the molar ratio increases from 2:1 to 12:1. It shows that excessive proportion of ferrous ions has a negative effect on the removal of Cu ions.

3.3 Effect of Stirring Time and Initial pH

The effects of stirring time and initial pH are show in Figure 3. Figure 3 a shows that with the increases of the stirring time, the removal rates of PO_4–P and Cu ions continue to increase until they stabilize at about 99.0% and 76.6%, respectively. When stirred for 20 min, the removal rate of PO_4–P reaches an equilibrium value, while it takes 30 min for Cu ions.

The effect of initial pH is investigated at 3.0, 4.0, 5.1, 5.6, 6.4, 7.6, 10.6, 11.7, and 12.4, respectively, and the result is shown in Figure 3 b. For the PO_4–P, the removal rate increases with the increase of pH in the ranges of 3.0 to 6.4. During the ranges of 6.4 to 10.6, the removal rate is stable about 99.0%. As the pH continues to rise, the removal rate of PO_4–P begins to decrease. When the initial pH reaches 12.4, the removal rate of PO_4–P drops to 35.0%. It may be due to the competition between phosphate and hydroxide. Specifically, in this high pH range, there are too many hydroxide ions, and calcium and iron ions are bound by hydroxide ions, reducing their binding with phosphate ions, resulting in a decrease in phosphorus removal rate.

The removal rate of Cu ions is positively correlated with pH in the selected pH range, and the removal rate increases from 8.0% to about 99.0% as the initial pH increases from 3.0 to 12.4. It is reasonable that the alkaline environment is conducive to the precipitation of Cu ions.

For a typical water containing 1 mM PO_4–P and 1 mM Cu ions with initial pH at 7.6, the optimized operating conditions as (Ca+Fe)/(P+Cu) molar ratio of 5:1, Ca/Fe molar ratio of 4:1, and 30-min stirring time are proposed. Under the as-described conditions, both of the removal rates of PO_4–P and Cu ions are close to 100%. Specifically, the residual concentration of PO_4–P in solution is less than 0.01 $mg{\cdot}L^{-1}$ and that of Cu ions 0.05 $mg{\cdot}L^{-1}$. It is confirmed that the co-removal of PO_4–P and Cu ions is effective and feasible by using $CaMg(CO_3)_2$ and $FeSO_4$ together. Additionally, the pH of the treated solution is finally stabilized at 7.0. More importantly, the moisture content of filter residue from $CaMg(CO_3)_2$–$FeSO_4$ process is about 70%.

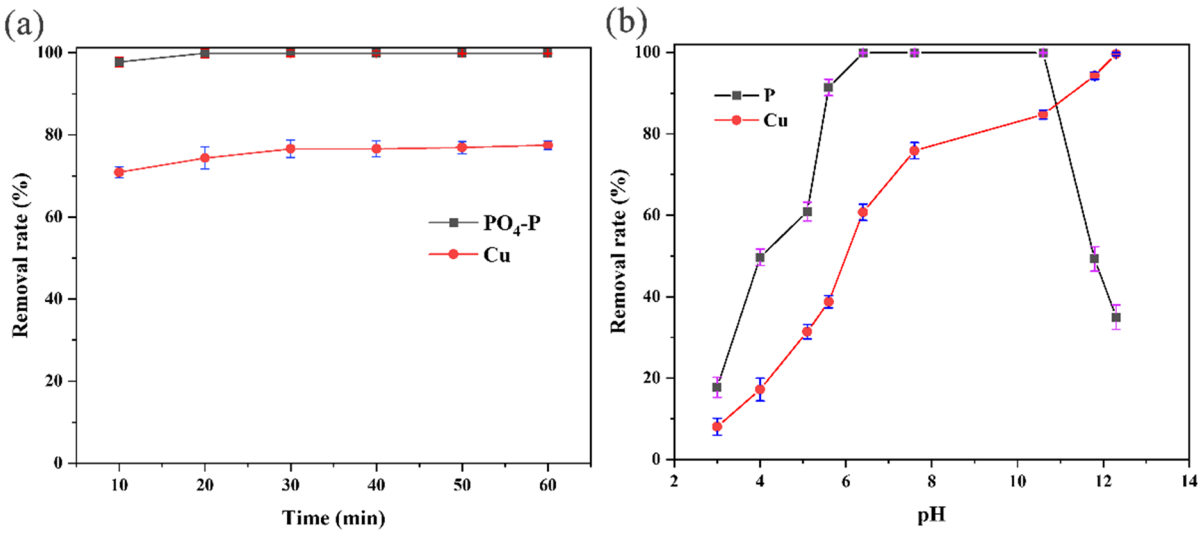

Figure 3 Effects of stirring time (**a**) and initial pH (**b**) on the removal rates of PO_4–P and Cu ions

3.4 Mechanism Discussion

The removal of PO_4–P by pure $CaMg(CO_3)_2$, pure $FeSO_4$, and the mixtures of them was investigated under the conditions as follows: 1 mM PO_4–P solutions were treated with $CaMg(CO_3)_2$–$FeSO_4$, pure $FeSO_4$, and pure $CaMg(CO_3)_2$, respectively. For the $CaMg(CO_3)_2FeSO_4$ process, the molar ratios of Fe/PO_4–P and Ca/Fe were respectively set at 1:1 and 1.5:1. For the cases of pure $FeSO_4$ and pure $CaMg(CO_3)_2$, the molar ratios of Fe/PO_4–P and Ca/PO_4–P were both at 2:1. All the samples were stirred for 30 min with the rotational speed of 500 rpm in beakers. The disposable filters with pore sizes of 0.22 μm were used for pre-treatment. The results are shown in Figure 4. It shows that the $CaMg(CO_3)_2$–$FeSO_4$ process can effectively remove PO_4–P, while the pure $CaMg(CO_3)_2$ process has little effect on the removal of PO_4–P. It is demonstrated that the $CaMg(CO_3)_2$ particles can greatly enhance the removal of PO_4–P by $FeSO_4$. The reason may lie in two ways: (i) the $CaMg(CO_3)_2$ particle provides a carrier for the aggregation of Fe–P compounds; (ii) the Ca ions on the surface of $CaMg(CO_3)_2$ particles may participate in the reaction process to form Fe-Ca-P complex.

The phase of the precipitate from PO_4–P removal using $CaMg(CO_3)_2$–$FeSO_4$ process is determined by an X-ray diffractometer. Figure 5 a shows the peaks of the sample are typical for calcite (PDF#05-0586). Figure 5 b shows the functional groups of the precipitate.

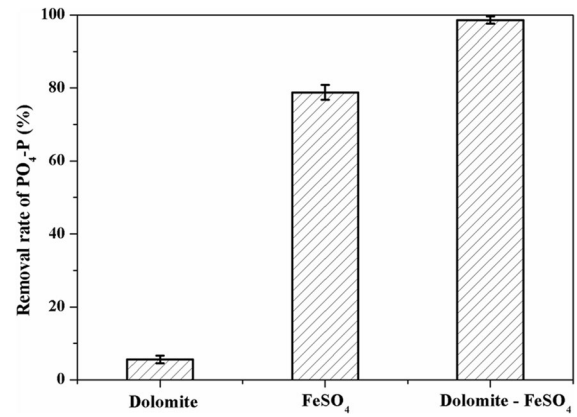

Figure 4 Removal rates of PO_4–P by using pure $CaMg(CO_3)_2$, pure $FeSO_4$, and $CaMg(CO_3)_2$–$FeSO_4$, respectively

The bands around the range of 3320–3600 cm^{-1} are assigned to the stretching and asymmetric stretching of hydroxyl groups. Another absorption peak around 1636 cm^{-1} corresponds to the stretching vibration of OH groups. The peaks at 1413, 872, and 711 cm^{-1} are assigned to $CaMg(CO_3)_2$ (Abdul Khalil et al. 2018, Ramasamy et al. 2018). The absorption peaks at 1008 and 550 cm^{-1} are attributed to the stretching vibration of P–O bond in PO_4^{3-} and the symmetrical bending vibration of P–O bond in PO_4^{3-}, respectively (Ramasamy et al. 2018). The results confirm that the PO_4–P is removed as amorphous substances.

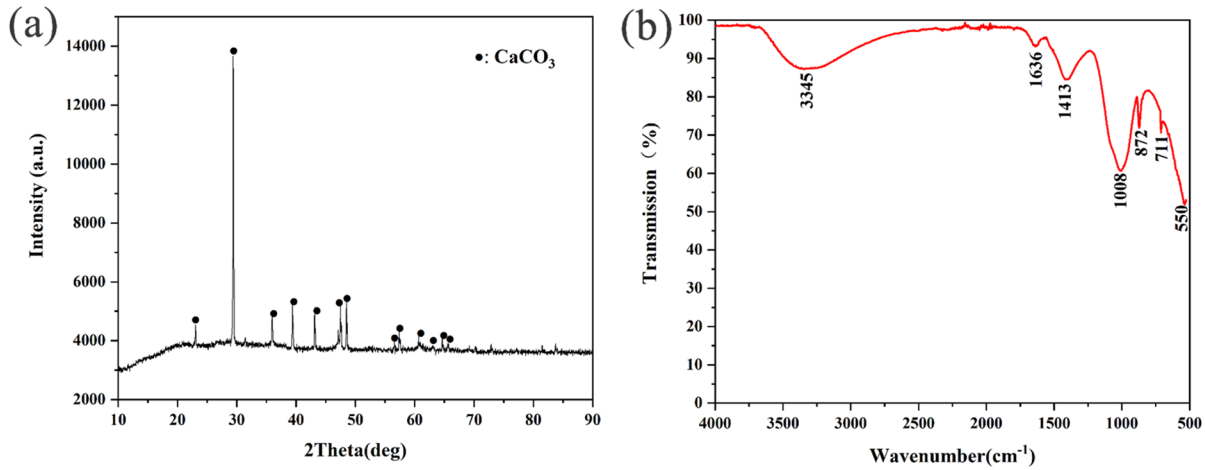

Figure 5 XRD pattern (**a**) and FTIR (**b**) of the precipitate obtained from PO_4–P removal by $CaMg(CO_3)_2$–$FeSO_4$

The raw $CaMg(CO_3)_2$ particles are hexagonal columnar and rhombohedral shape as shown in Figure 6 a and b. The morphological features of the particles eroded by Cu ions are shown in Figure 6 c and d, demonstrating that the raw $CaMg(CO_3)_2$ is corroded deeply by Cu ions and the crystal is peeled off into a sheet along the cleavage plane, resulting in the production of flaky particles. The raised spots are found at the marked positions (red numbers 1, 2, and 3) on the surface of flakes, which are probably due to the corrosion and deposition of Cu ions on $CaMg(CO_3)_2$. It is noteworthy that the flaky particles have two-dimensional nanostructured as shown in Figure 6 c. The two-dimensional nanostructured is conducive to increase the contact area of particles with ions in solution, improving the chemical reactivity and

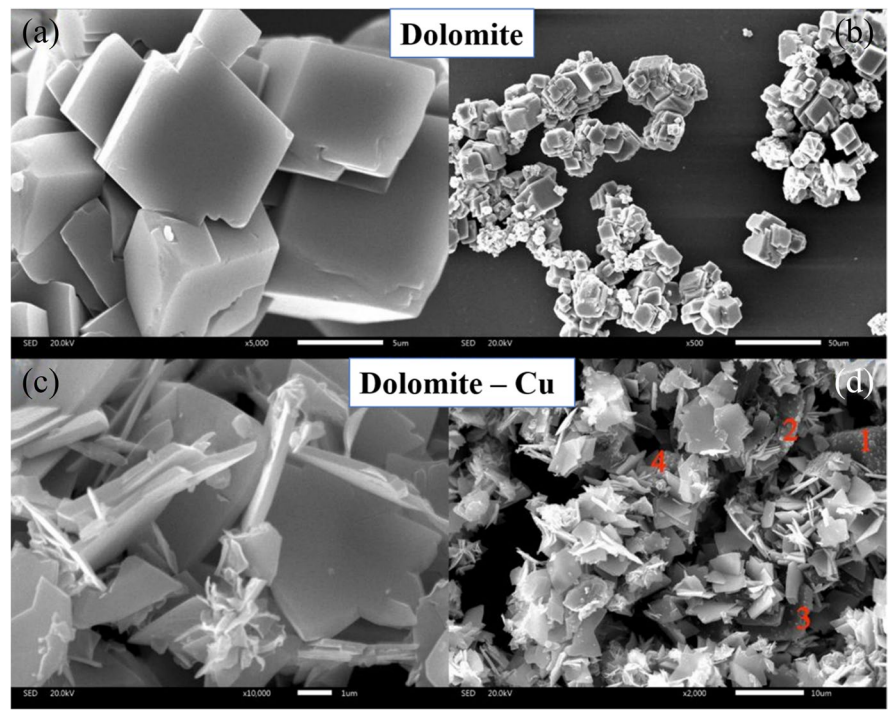

Figure 6 SEM images of the raw $CaMg(CO_3)_2$ (**a**, **b**) and the precipitate generated by stirring $CaMg(CO_3)_2$ and $CuSO_4$ (**c**, **d**). Conditions: 100 mg $CaMg(CO_3)_2$ was added to 100 mL $CuSO_4$ solution with copper concentration of 200 mg·L^{-1} and stirred by a magnetic stirrer at 200 rpm for 240 min

adsorption. The Cu ions may promote the PO_4–P removal in the $CaMg(CO_3)_2$–$FeSO_4$ process.

The concentration of Cu in solution is detected after stirring with $CaMg(CO_3)_2$ for 240 min. As shown in Figure 7 a, the concentration of Cu decreases from 200 to 0.5 mg·L^{-1} with the stirring time increase from 0 to 240 min. The phase of the precipitate from stirring $CuSO_4$ solution with $CaMg(CO_3)_2$ is analyzed by the X-ray diffractometer as shown in Figure 7 b. The peaks of posnjakite ($Cu_4(OH)_6SO_4{\cdot}2H_2O$, PDF#43-0670) and calcite (PDF#05-0586) are found in the sample, indicating that Cu ions are removed in the form of $Cu_4(OH)_6SO_4{\cdot}2H_2O$ by using pure $CaMg(CO_3)_2$.

3.4.1 *Effect of Cu on the PO_4–P Removal*

As discussed above, the Cu ions may promote the PO_4–P removal in the $CaMg(CO_3)_2$–$FeSO_4$ process. Thus, the effect of Cu ions on the PO_4–P removal is investigated in the processes of pure $CaMg(CO_3)_2$ (as Figure 8). For the pure $CaMg(CO_3)_2$ process, the removal rate of PO_4–P is only 5.03%. After adding 0.5 mM Cu ions, the removal rate increases to 26.1%. In the process of $CaMg(CO_3)_2$–$FeSO_4$, the removal rate of PO_4–P increases from 82.2 to 93.1% with the addition of Cu ions. It is confirmed that the Cu ions can promote the PO_4–P removal in the processes, as Cu ions peel off massive dolomite into nanosheets with high surface energy, thereby improving the removal rate of PO_4–P.

The phase of the sediment from the co-removal of PO_4–P and Cu is shown in Figure 9. The rough line indicates that PO_4–P and Cu are removed in form of an amorphous precipitate with low solubility. As shown in Fig.10, in the process of treatment, the raw $CaMg(CO_3)_2$ particles

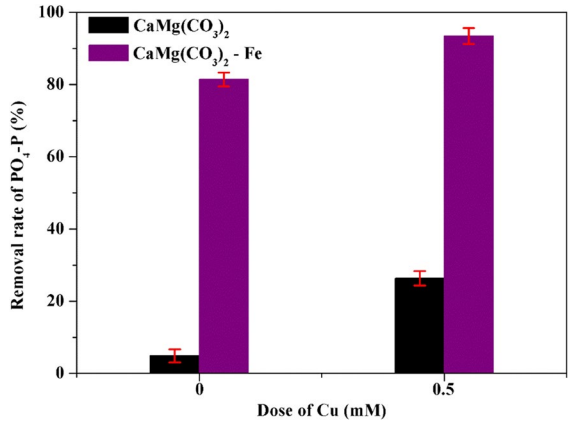

Figure 8 Effect of Cu ions on the PO_4–P removal. Conditions: 0.5 mM $CuSO_4$ were added into 200 mL solution with 1 mM PO_4–P and stirring with 0.2 mmol $CaMg(CO_3)_2$ and 0.4 mmol $CaMg(CO_3)_2$–$FeSO_4$ (Fe/Ca = 1:1) for 30min, respectively

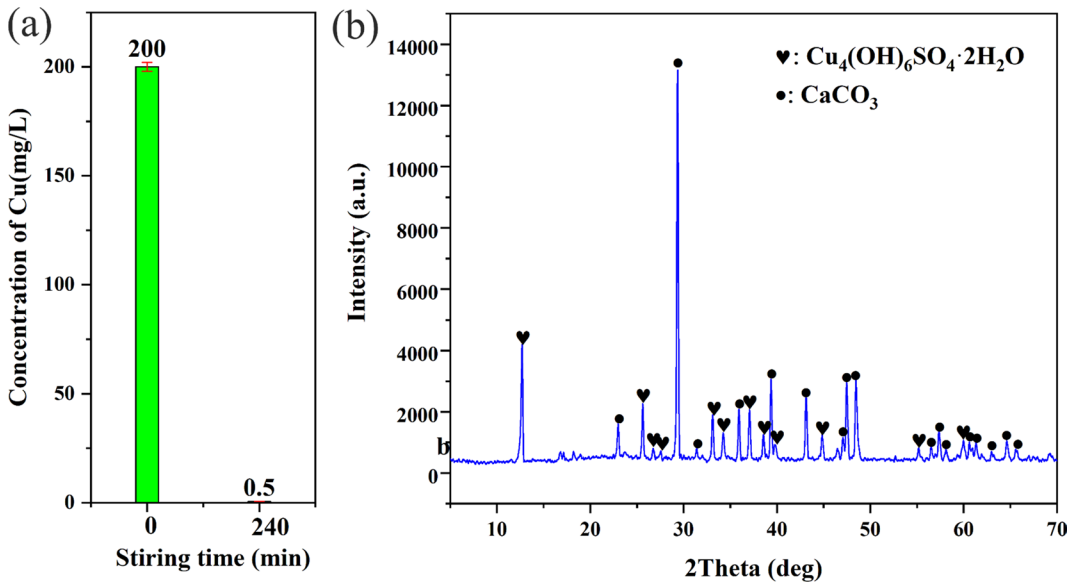

Figure 7 Concentration of Cu before and after stirring with $CaMg(CO_3)_2$ (**a**) and XRD pattern of the precipitate. Conditions: 100 mg $CaMg(CO_3)_2$ was added to 100 mL $CuSO_4$ solution with copper concentration of 200 mg·L^{-1} and stirred by a magnetic stirrer at 500 rpm for 240 min

with hexagonal columnar shape are attacked by Fe^{2+} and Cu^{2+} in aqueous solution, peeled along the cleavage plane, and transformed into dolomite nanosheets. A portion of the Ca^{2+} ions in raw $CaMg(CO_3)_2$ structure are exchanged by Fe^{2+} and Cu^{2+} ions, and turn into free Ca^{2+} ions in aqueous solution, accompanied by the fixing of Cu ions. The hydrolysis of CO_3^{2-} on the surface of the $CaMg(CO_3)_2$ particle generates OH^- ions and free Ca^{2+} ions. The Fe^{2+} ions can be easily oxidized to Fe^{3+} in the present of dissolved oxygen (DO) and OH^- (Zhang et al. 2019). The co-precipitation of free Ca^{2+}, Fe^{3+}, and PO_4^{3-} ions occurs quickly in the presence of $CaMg(CO_3)_2$ sheets with the stirring operation.

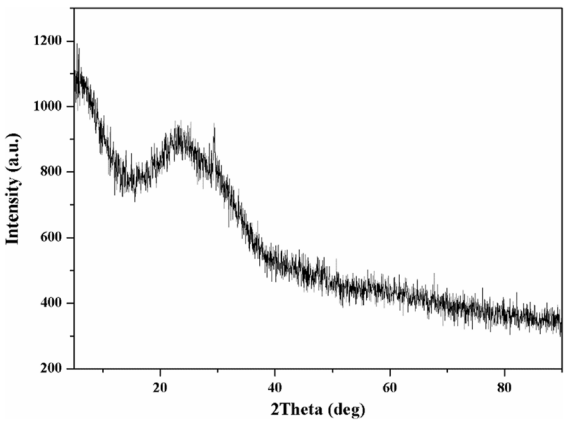

Figure 9 XRD pattern of the sediment produced by the co-removal of PO–P and Cu using $CaMg(CO_3)_2$–$FeSO_4$ process

4 Conclusions

The completely synchronous removal of PO_4–P and Cu ions can be achieved by the $CaMg(CO_3)_2$–$FeSO_4$ process. The main influencing factors include the dosage of $CaMg(CO_3)_2$ and $FeSO_4$, the molar ratio of Ca and Fe, the stirring time, and the initial pH. Under suitable conditions, for example, the Ca to Fe molar ratio is equal to 4:1, the Fe to P+Cu molar ratio is equal to 1:1, the initial pH at 5.6–10, and the stirring time is 30 min, and the removal rates of PO_4–P and Cu ions are nearly 99%. The presence of Fe is critical for the removal of PO_4–P, and the PO_4–P is mainly removed by forming insoluble amorphous precipitate. The raw $CaMg(CO_3)_2$ is susceptible to corrosion by Cu ions and resulting in the production of flaky particles, which have two-dimensional nanostructured. The two-dimensional nanostructured is conducive to increase the contact area of particles with ions in solution, improving the chemical reactivity and adsorption. The $CaMg(CO_3)_2$ is essential for the Cu removal and the Cu is mainly removed in the form of posnjakite ($Cu_4(OH)_6SO_4{\cdot}2H_2O$) by the pure $CaMg(CO_3)_2$ process. However, in the $CaMg(CO_3)_2$–$FeSO_4$ process, the P and Cu are removed by forming an amorphous precipitate.

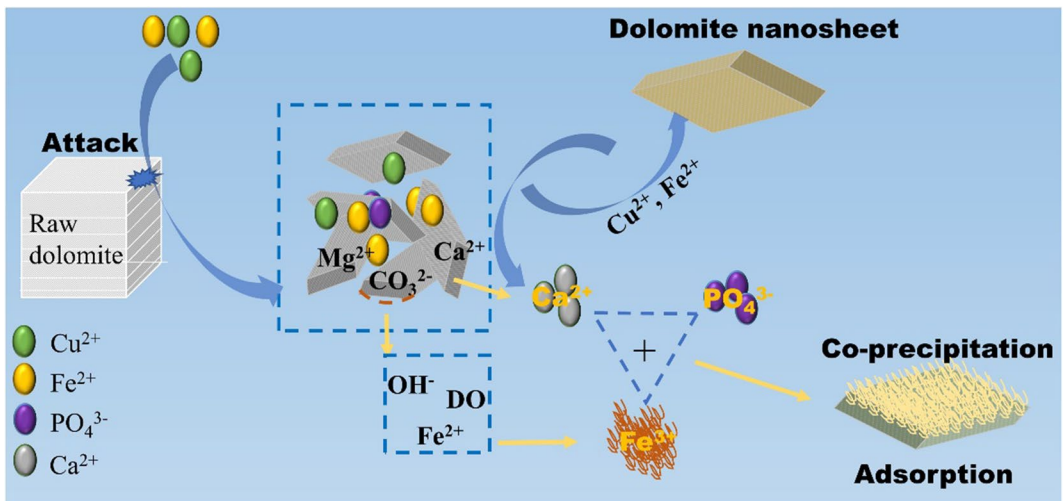

Figure 10 Schematic diagram of the reaction mechanism

Data Availability The data that support the findings of this study are available from the corresponding author upon reasonable request.

Declarations

Conflict of Interest The authors declare that no competing interests.

References

Abdul Khalil, H. P. S., Chong, E. W. N., Owolabi, F. A. T., Asniza, M., Tye, Y. Y., Tajarudin, H. A., Paridah, M. T., & Rizal, S. (2018). Microbial-induced CaMg(CO3)2 filled seaweed-based film for green plasticulture application. *Journal of Cleaner Production, 199*, 150–163.

Awual, M. R. (2019). Efficient phosphate removal from water for controlling eutrophication using novel composite adsorbent. *Journal of Cleaner Production, 228*, 1311–1319.

Badsha, M. A. H., & Lo, I. M. C. (2020). An innovative pH-independent magnetically separable hydrogel for the removal of Cu(II) and Ni(II) ions from electroplating wastewater. *Journal of Hazardous Materials, 381*, 121000.

Chen, D., Zhang, C., Rong, H., Zhao, M., & Gou, S. (2020). Treatment of electroplating wastewater using the freezing method. *Separation and Purification Technology, 234*, 116043.

Clark, T., Stephenson, T., & Pearce, A. (1997). Phosphorus removal by chemical precipitation in a biological aerated filter. *Water Research, 31*(10), 2557–2563.

Fu, F. L., & Wang, Q. (2011). Removal of heavy metal ions from wastewaters: A review. *Journal of Environmental Management, 92*(3), 407–418.

Guo, Z., Li, J., Guo, Z., Guo, Q., & Zhu, B. (2017). Phosphorus removal from aqueous solution in parent and aluminum-modified eggshells: Thermodynamics and kinetics, adsorption mechanism, and diffusion process. *Environmental Science and Pollution Research International, 24*(16), 14525–14536.

Lan, S., Ju, F., & Wu, X. (2012). Treatment of wastewater containing EDTA-Cu(II) using the combined process of interior microelectrolysis and Fenton oxidation–coagulation. *Separation and Purification Technology, 89*, 117–124.

Lei, Y., Narsing, S., Saakes, M., van der Weijden, R. D., & Buisman, C. J. N. (2019). Calcium carbonate packed electrochemical precipitation column: New concept of phosphate removal and recovery. *Environmental Science & Technology, 53*(18), 10774–10780.

Li, X., Zhang, Q., & Yang, B. (2020). Co-precipitation with CaMg(CO3)2 to remove heavy metals and significantly reduce the moisture content of filter residue. *Chemosphere, 239*, 124660.

Liang, S., Zheng, W., Zhu, L., Duan, W., Wei, C., & Feng, C. (2019). One-step treatment of phosphite-laden wastewater: A single electrochemical reactor integrating superoxide radical-induced oxidation and electrocoagulation. *Environmental Science & Technology, 53*(9), 5328–5336.

Liu, Y., Shi, H., Li, W., Hou, Y., & He, M. (2011). Inhibition of chemical dose in biological phosphorus and nitrogen removal in simultaneous chemical precipitation for phosphorus removal. *Bioresource Technology, 102*(5), 4008–4012.

Morse, G. K., Brett, S. W., Guy, J. A., & Lester, J. N. (1998). Review: Phosphorus removal and recovery technologies. *Science of The Total Environment, 212*(1), 69–81.

Qi, Y., Thapa, K. B., & Hoadley, A. F. A. (2011). Application of filtration aids for improving sludge dewatering properties – A review. *Chemical Engineering Journal, 171*(2), 373–384.

Ramasahayam, S. K., Guzman, L., Gunawan, G., & Viswanathan, T. (2014). A comprehensive review of phosphorus removal technologies and processes. *Journal of Macromolecular Science A, 51*(6), 538–545.

Ramasamy, V., Anand, P., & Suresh, G. (2018). Synthesis and characterization of polymer-mediated CaMg(CO3)2 nanoparticles using limestone: A novel approach. *Advanced Powder Technology, 29*(3), 818–834.

Wang, H., Dong, W., Li, T., & Liu, T. (2015). A modified BAF system configuring synergistic denitrification and chemical phosphorus precipitation: Examination on pollutants removal and clogging development. *Bioresource Technology, 189*, 44–52.

Zhang, J., Bligh, M. W., Liang, P., Waite, T. D., & Huang, X. (2018). Phosphorus removal by in situ generated Fe(II): Efficacy, kinetics and mechanism. *Water Resources., 136*, 120–130.

Zhang, T., Zhao, Y., Kang, S., Li, Y., & Zhang, Q. (2019). Formation of active $Fe(OH)_3$ in situ for enhancing arsenic removal from water by the oxidation of Fe(II) in air with the presence of CaMg(CO3)2. *Journal Cleaner Production, 227*, 1–9.

Zhou, K., Wu, B., Su, L., Gao, X., Chai, X., & Dai, X. (2017). Development of nano-CaO_2-coated clinoptilolite for enhanced phosphorus adsorption and simultaneous removal of COD and nitrogen from sewage. *Chemical Engineering Journal, 328*, 35–43.